# MinC, MinD, and MinE Drive Counter-oscillation of Early-Cell-Division Proteins Prior to *Escherichia coli* Septum Formation

**Paola Bisicchia,[a] Senthil Arumugam,[b] Petra Schwille,[c] David Sherratt[a]**

Department of Biochemistry, University of Oxford, Oxford, United Kingdom[a]; Institute Curie, Paris, France[b]; Max Planck Institute of Biochemistry, Martinsried, Germany[c]

**ABSTRACT** **Bacterial cell division initiates with the formation of a ring-like structure at the cell center composed of the tubulin homolog FtsZ (the Z-ring), which acts as a scaffold for the assembly of the cell division complex, the divisome. Previous studies have suggested that the divisome is initially composed of FtsZ polymers stabilized by membrane anchors FtsA and ZipA, which then recruit the remaining division proteins. The MinCDE proteins prevent the formation of the Z-ring at poles by oscillating from pole to pole, thereby ensuring that the concentration of the Z-ring inhibitor, MinC, is lowest at the cell center. We show that prior to septum formation, the early-division proteins ZipA, ZapA, and ZapB, along with FtsZ, assemble into complexes that counter-oscillate with respect to MinC, and with the same period. We propose that FtsZ molecules distal from high concentrations of MinC form relatively slowly diffusing filaments that are bound by ZapAB and targeted to the inner membrane by ZipA or FtsA. These complexes may facilitate the early stages of divisome assembly at midcell. As MinC oscillates toward these complexes, FtsZ oligomerization and bundling are inhibited, leading to shorter or monomeric FtsZ complexes, which become less visible by epifluorescence microscopy because of their rapid diffusion. Reconstitution of FtsZ-Min waves on lipid bilayers shows that FtsZ bundles partition away from high concentrations of MinC and that ZapA appears to protect FtsZ from MinC by inhibiting FtsZ turnover.**

**IMPORTANCE** **A big issue in biology for the past 100 years has been that of how a cell finds its middle. In *Escherichia coli*, over 20 proteins assemble at the cell center at the time of division. We show that the MinCDE proteins, which prevent the formation of septa at the cell pole by inhibiting FtsZ, drive the counter-oscillation of early-cell-division proteins ZapA, ZapB, and ZipA, along with FtsZ. We propose that FtsZ forms filaments at the pole where the MinC concentration is the lowest and acts as a scaffold for binding of ZapA, ZapB, and ZipA: such complexes are disassembled by MinC and reform within the MinC oscillation period before accumulating at the cell center at the time of division. The ability of FtsZ to be targeted to the cell center in the form of oligomers bound by ZipA and ZapAB may facilitate the early stages of divisome assembly.**

**Received** 7 October 2013 **Accepted** 18 November 2013 **Published** 10 December 2013

**Citation** Bisicchia P, Arumugam S, Schwille P, Sherratt D. 2013. MinC, MinD, and MinE drive counter-oscillation of early-cell-division proteins prior to *Escherichia coli* septum formation. mBio 4(6):e00856-13. doi:10.1128/mBio.00856-13.

**Editor** Susan Gottesman, National Cancer Institute



Address correspondence to David Sherratt, david.sherratt@bioch.ox.ac.uk.

The first known event in bacterial cytokinesis is the polymerization of the tubulin homologue FtsZ into a ring-like structure, the Z-ring, assembled on the cytoplasmic face of the cell membrane at the future site of cell constriction and stabilized by the membrane-anchoring proteins ZipA and FtsA (1). Assembly of the Z-ring is regulated temporally and spatially, to ensure that it occurs at the correct time of the cell cycle and in the correct place, between segregated chromosomes at the center of the cell. Two negative regulatory systems have been identified in *Escherichia coli*: the nucleoid occlusion (NO) system, which prevents Z-ring formation over the nucleoid, and the Min system, which inhibits cell division away from midcell. The NO system is mediated through DNA binding protein SlmA, which binds to regions scattered in the origin-proximal two-thirds of the chromosome (2) and prevents Z-ring formation through direct interaction with FtsZ (3, 4): as the duplicating chromosomes segregate, SlmA moves away from midcell, making it permissive for Z-ring assembly. The Min system comprises three proteins, MinC, MinD, and MinE. MinC dimer binding to FtsZ protofilaments directly or indirectly leads to FtsZ bundle and protofilament disassembly by shortening of FtsZ polymers and by competing with FtsA/ZipA for the binding to the C terminus of FtsZ (5–8). MinC is recruited to the cell membrane by MinD and is topologically regulated by MinE, which undergoes an oscillation along with MinC and MinD between the poles of the cell (reviewed in reference 9). This oscillation is such that the time-averaged concentration of the cell division inhibitor MinC is lowest at the cell center and highest at the poles (10), with the effect of blocking cell division at poles and allowing it at the cell center.

The mature cell division machinery comprises over 24 different protein components (11). Such proteins are recruited to midcell following a clear pattern of genetic dependencies, which does not necessarily reflect the temporal order of assembly (12). The current view is that the divisome is initially composed of membrane-anchored FtsZ polymers, which subsequently recruit other cell division proteins (12, 13), with a subset of early-division

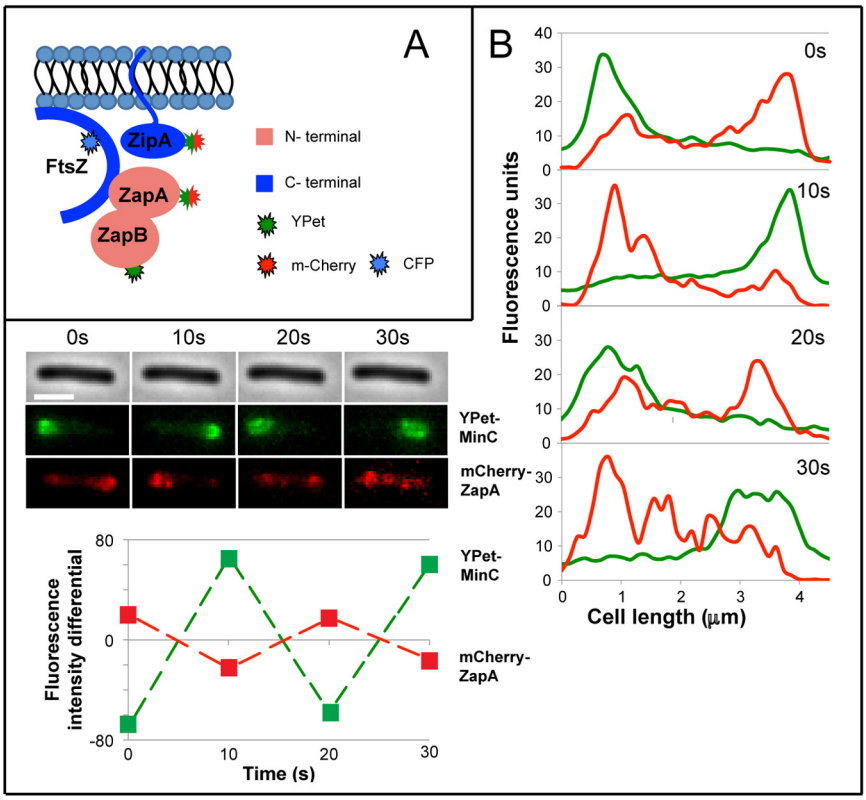


**FIG 1** (A) Schematic presentation of constructs generated for creating YPet, mCherry, and CFP derivatives of early-cell-division proteins. Fusion proteins were expressed at their native chromosomal location under the control of their physiological promoter, with the exception of FtsZ-CFP, which was expressed from a plasmid at low levels. YPet, mCherry, and CFP fluorophores were fused to either the C terminus or the N terminus of the protein, as illustrated. (B) The panel at center left shows a time-lapse analysis of *E. coli* strain PB213 (yPet-minC mCherry-zapA). A representative elongating cell is displayed. The graph below the panel represents the plot of differential fluorescence intensities between the left side and right side of each cell. Graphs on the right display the line profiles of fluorescent signals emanating from the cell. Arbitrary fluorescent units (obtained with the ImageJ software) are plotted on the *y* axis; cell length (in $\mu$m) is plotted on the *x* axis. Cells were grown in M9 medium supplemented with 0.2% glycerol at 37°C. Bars, 2 $\mu$m.

proteins, including ZapA and ZapB, being recruited before the majority of divisome components (Fig. 1) (14).

ZipA is an integral membrane protein that, together with FtsA, plays the essential role of tethering the Z-ring to the inner membrane by directly interacting with FtsZ filaments (15). In addition, ZipA is capable of inducing FtsZ bundling *in vitro* (16, 17) and of protecting FtsZ from degradation by ClpP (18), consistent with a role in stabilization of the Z-ring. The ZapA cytoplasmic protein, like ZipA, apparently stabilizes both protofilaments and bundles (19–23). Unlike ZipA and ZapA, the ZapB cytoplasmic protein does not bind FtsZ directly but is recruited to the Z ring through ZapA (24); it has been implicated in stimulation of Z-ring formation (25) as well as in coordination of cell division with chromosome segregation through its direct interaction with MatP, a protein that binds to the terminus region of the chromosome, promoting its compaction and organization (26, 27).

The *in vivo* dynamics and localization of early-cell-division proteins have so far been investigated only in relation to their septal location, where they have been observed to localize approximately simultaneously (19, 28–30). However, these studies were conducted using fluorescent derivatives expressed under conditions of inducible control and in addition to the wild-type copy of the protein and therefore effectively under conditions of overexpression (15, 19, 24, 25, 31). In order to assess the dynamics of such proteins under more physiological conditions, we expressed fluorescent versions of these proteins at their original chromosomal loci under the control of their native promoter. We found that the bulk cellular fluorescence of functional ZapA, ZapB, and ZipA fluorescent fusions exhibited an oscillatory movement in the direction opposite to that of MinC and in the same direction and with the same periodicity as that of bulk FtsZ. Although we could not study the movement of FtsA because of the lack of a functional fusion protein, our expectation is that FtsA undergoes a similar oscillatory movement. The oscillation of ZipA, ZapA, and ZapB was dependent on Min and on the presence of FtsZ filaments, since it was prevented in a *minDE* null mutant strain, as well as upon overexpression of SulA, which prevents FtsZ polymerization.

We propose that FtsZ starts forming short filaments in the cytoplasm before cell division; such filaments are immediately decorated by ZapAB and ZipA, targeted to the cell membrane through ZipA and FtsA, and disassembled by MinC, ensuring that Z-rings, containing bundles of FtsZ protofilaments, form only at the cell center. The ability of early-cell-division proteins to start associating with FtsZ before cell division represents an efficient mechanism for the cell for rapid assembly of the Z-ring.

## RESULTS AND DISCUSSION

**ZapAB, ZipA, and FtsZ display a counter-oscillation with respect to MinC within cells.** In order to determine the patterns of localization of ZapA, ZapB, and ZipA in cells, we used functional fluorescent mYPet and mCherry fusions of these proteins, expressed from their endogenous promoters in the *E. coli* chromosome (Fig. 1A). Strains expressing single-fusion proteins, or combinations, grew with normal length and division characteristics and did not display any noticeable cell growth and morphology defects. In addition, the fusion proteins correctly localized to septa at the expected time within the cell cycle, indicating that the presence of the fluorophores did not affect their function.

To visualize multiple cell division proteins in the same cell, we constructed strains expressing all possible combinations of two of the three proteins ZapA, ZapB, and ZipA, with one protein fluorescing in the green channel and the other in the red channel. In addition, to determine the localization of these proteins with respect to FtsZ, we transformed such strains with plasmid pCP8, which allows constitutive expression of an FtsZ-cyan fluorescent protein (CFP) derivative from a weak promoter. Previous work

has shown that in cells carrying this plasmid, about 11% of the total FtsZ is the FtsZ-CFP fluorescent version and that these cells grow normally and do not have aberrant FtsZ-ring structures (32).

Cells of these strains growing in minimal medium showed fluorescent signals at septa, as expected. In addition, elongating cells with no septal signal displayed bulk fluorescence distributed nonuniformly throughout the cell as well as brighter nonseptal spots (see Fig. S1 in the supplemental material). Time-lapse analysis showed that ZapA, ZapB, ZipA, and FtsZ are targeted at the septum within 1 min of each other (see Movie S1 in the supplemental material). We also noted in the initial time-lapse experiments that the localization of the nonseptal signals changed over time (see Movie S2 in the supplemental material). To investigate further the dynamic behavior of ZipA, ZapA, and ZapB, time-lapse images were acquired every 10 s, using a 200-ms capture time for mYPet and a 500-ms capture time for mCherry. Analysis showed an oscillation-like movement of a large fraction of the total fluorescence along the long axis of the cell. This oscillatory behavior was readily observed in about 50% of cells for all strains analyzed. A complete cycle took about 20 s (see the ZapA-, ZapB-, and ZipA-derived signals in Fig. 1B; see also Fig. S1). This dynamic behavior was strikingly similar to that of the MinCDE proteins, which have an oscillation cycle with a periodicity which was found to range between seconds and minutes, depending on the growth conditions (see reference 33 and references therein).

We then compared the apparent oscillation of ZipA-ZapAB-FtsZ with that of MinC, using functional YPet and mCherry fusions of MinC expressed from the endogenous promoter. Time-lapse analysis showed the expected oscillation of MinC in all cells, with a periodicity of about 20 s, similar to that observed for the early-division proteins (see Movie S3 in the supplemental material). Simultaneous time-lapse observations of MinC with ZapA showed counter-oscillation of MinC, with ZapA in all cells that exhibited ZapA oscillation (Fig. 1B). The oscillatory behavior was evident in elongating and dividing cells (Fig. 1B; see also Fig. S1 in the supplemental material). Quantitative analysis of the differential fluorescent intensities between the left and right sides of the cell for both YPet-MinC- and mCherry-ZapA-derived signals highlights the oscillation behavior of MinC and ZapA and shows that such oscillation occurred both in elongating cells and, although to a lesser extent, in cells in which the septum is already forming (see Fig. S1). Linescan analysis confirmed the counter-oscillatory behavior (Fig. 1B). The same result was obtained when MinC and ZipA ZipA or ZapB dynamics were compared (see Fig. S1).

To test whether we could compare any FtsZ oscillation to that of ZipA or ZapAB, we used cells expressing an FtsZ-CFP derivative under the control of a weak promoter on a low-copy-number plasmid in cells that had a normal endogenous *ftsZ* gene (32). These cells also expressed ZipA-YPet, YPet-ZapA, or YPet-ZapB. The time-lapse analysis shows that FtsZ co-oscillated with ZipA-ZapAB in all cells that exhibited ZipA-ZapAB oscillation (Fig. 2; see also Fig. S2 in the supplemental material). An earlier study (34) had also reported counter-oscillation of FtsZ with MinC, but in those experiments it was observed in only a small fraction of long cells, perhaps because their experiments used FtsZ-green fluorescent protein (GFP) expressed from an ectopic gene under the control of an IPTG (isopropyl-β-D-thiogalactopyranoside)-inducible promoter in a wild-type *ftsZ* background, thereby resulting in a fraction of cellular FtsZ being fused to fluorescent protein that was larger than that seen here.

Taken together, these results show that ZapAB, ZipA, and FtsZ co-oscillate in the opposite direction with respect to MinC, and with similar periodicity, consistent with ZapAB-ZipA being complexed to FtsZ prior to its recruitment to midcell.

**ZapA, ZapB, and ZipA oscillation is lost in Min$^-$ cells.** To test our expectation that the FtsZ-ZipA-ZapAB co-oscillation would be dependent on a functional Min system, we analyzed the dynamic behavior of these proteins in cells lacking Min (Min$^-$ cells). Previous work had already showed that FtsZ oscillation is MinCDE dependent (34). We found that, although these proteins still appeared to associate in complexes in Min$^-$ cells, the oscillatory behavior was lost in all cells, demonstrating that ZipA-ZapAB counter-oscillation is MinCDE dependent (Fig. 2B; see also Fig. S3 in the supplemental material).

**ZapB oscillation is ZapA dependent.** Since ZapA binds FtsZ and ZapB binds ZapA, we predicted that if the counter-oscillatory behavior requires FtsZ oligomers as a scaffold, then ZapB oscillation would be ZapA dependent. This was indeed the case; Δ*zapA* cells showed no ZapB oscillation but retained FtsZ oscillation, despite Δ*zapA* cells being longer and having division defects and misplaced Z-rings (Fig. 2C) (24). We propose that the polar ZapB spot present in most elongating cells of the Δ*zapA* strain results from interactions of ZapB and MatP-*ter*, which are pole proximal for most of the cell cycle (27, 32).

**SulA inhibition of FtsZ oligomerization prevents oscillation of ZapAB, ZipA, and FtsZ.** If FtsZ polymerization/bundling provides the "scaffold" for the observed counter-oscillation, then inhibition of FtsZ polymerization into protofilaments by SulA overexpression (35–37) should block the counter-oscillation of ZipA-ZapAB. This was the case; SulA overexpression prevented not only the oscillatory behavior of FtsZ but also that of ZipA-ZapAB (Fig. 3). In addition, SulA overexpression led to the loss of the nonseptal ZipA-ZapAB fluorescent spots that were observed in wild-type cells, consistent with the view that in wild-type cells the spots are composed of FtsZ filaments bound to ZapAB and ZipA. The regular spacing of fluorescent ZapAB "clouds" corresponded to nucleoid-free spaces (see Fig. S4 in the supplemental material), indicating that they were present in oligomeric assemblies that were excluded from the bulk nucleoid mass. This explanation is consistent with the ability of these proteins to form filaments *in vitro* (19–22, 24) and with the observation that, in contrast with ZapA and ZapB, the signal derived from FtsZ appeared homogeneous throughout the cell and therefore does not seem to be excluded from diffusing into the nucleoid (Fig. 3A). Similarly, the ZipA-YPet signal was present throughout the long axis of the cell, with some enrichment to the cell membrane (Fig. 3D; see also Fig. S4C and D in the supplemental material). The Min-dependent FtsZ oscillatory behavior observed previously was most readily observed in cells that were elongated by FtsZ or FtsI impairment or by SulA expression (34). We are not sure why SulA expression did not inhibit FtsZ oscillation in these experiments but note that cells were grown in rich medium and that the cellular level of FtsZ was increased by expressing an additional 30% to 40% of FtsZ as a fluorescent fusion. We propose that, under those conditions, there may have been insufficient SulA to sequester all of the FtsZ.

The results presented so far indicate that the counter-oscillation of ZipA and ZapAB is due to the rapid formation of

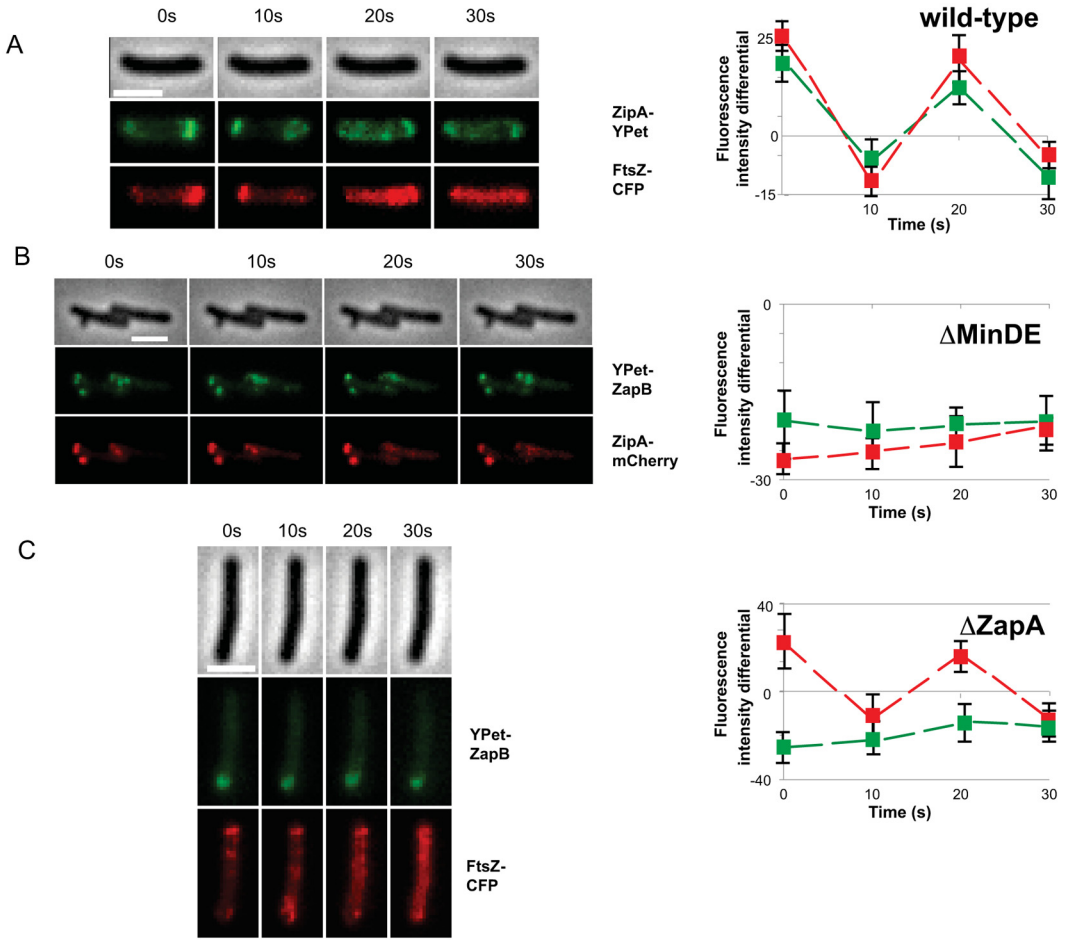


**FIG 2** Time-lapse analysis. Data are shown for PB283 (zipA-yPet $p_{ftsK}$ftsZ-cfp) (A), PB352 (*yPet-zapB zipA-mCherry* Δ*minDE*) (B), and PB393 PB393 (*yPet-zapB* $p_{ftsK}$*FtsZ-CFP* Δ*zapA*) (C). Fields of view containing >100 cells were examined, and 5 representative elongating cells were analyzed. Graphs represent the plot of differential fluorescence intensities between the left side and right side of each cell: the mean values for 5 different cells are reported at each time point, with error bars representing the standard deviations from the means. Cells were grown in M9 medium supplemented with 0.2% glycerol at 37°C. Bars, 2 μm.

FtsZ filaments, which are immediately decorated by early-cell-division proteins at the pole where the MinC concentration is lower and are rapidly disassembled when the MinC local concentration arises periodically. In this scenario, the formation of FtsZ filaments bound to ZipA-ZapAB would make the diffusion of these proteins slower and therefore more visible by epifluorescence microscopy. This model implies that FtsZ is able to assemble and turn over within the 20-s oscillation period of MinC; crucially, this is consistent with the rate of FtsZ turnover that has been measured *in vivo* for *E. coli* by fluorescence recovery after photobleaching (FRAP) analysis: recovery of a bleached spot on the FtsZ occurs with a half-time of about 9 s, indicating that FtsZ subunits in the Z-ring exchange with those in the cytoplasm on this time scale (38).

***In vitro*-reconstituted MinCDE waves exclude FtsZ bundles.** We wished to test whether we could recapitulate any aspects of the *in vivo* counter-oscillation that we characterized *in vitro* and to test whether ZapA had any effects on the dynamics. Min waves were established on supported lipid bilayers in the presence of purified FtsZ using established conditions (39, 40). FtsZ bundle networks were assembled using a mixture of wild-type FtsZ and FtsZ-YFP-MTS, which contains the membrane targeting sequence (MTS) from MinD (40). FtsZ-YFP-MTS polymerized on the supported lipid bilayer and formed a bundled dynamic network of mixed polymers containing FtsZ and FtsZ-YFP-MTS. The bundles were about 5 to 6 protofilaments thick and showed dynamic turnover because of ongoing GTP hydrolysis (40). The FtsZ bundles and Min waves were reconstituted as previously described (40, 41). Min waves were imaged using MinD-Cy5, which colocalizes with MinC and MinE (41). We observed that FtsZ bundles were subjected to the action of MinC in the Min waves, as visualized by FtsZ bundles being excluded from the zones containing Min, with FtsZ bundle assembly and disassembly occurring along the lipid support following the Min waves (Fig. 4A, top panel). In the absence of GTP, FtsZ filaments did not form; in the absence of MinC, or in the presence of the nonhydrolyzable GTP analog GMPCPP, the Min waves propagated through the FtsZ filaments (data not shown).

Since ZapA facilitates FtsZ bundling formation and protects FtsZ bundles from the inhibitory effect of MinC *in vitro* (42), we then tested the effect of adding ZapA to the dynamics of the system, in particular, to see if ZapA protected FtsZ bundles from the

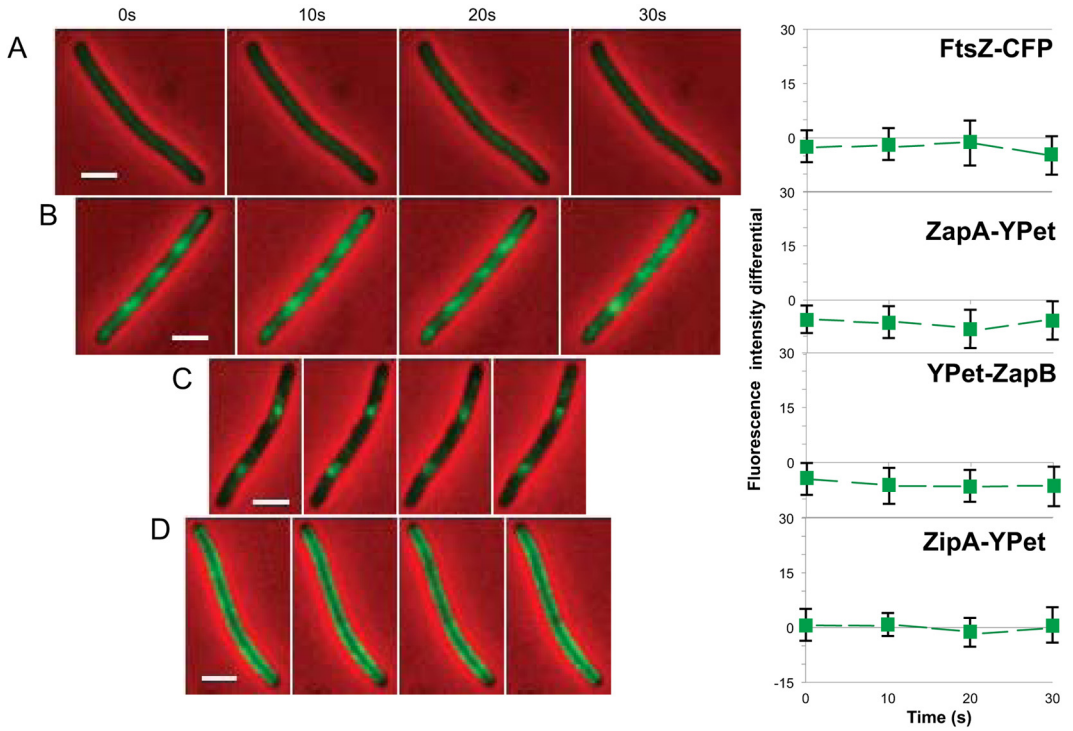


**FIG 3** Time-lapse analysis. Data are shown for PB253 ($p_{ara}$SulA $p_{ftsK}$ftsZ-*cfp*) (A), PB245 ($p_{ara}$sulA zapA-yPet) (B), PB323 ($p_{ara}$sulA yPet-zapB) (C), and ($p_{ara}$sulA zipA-yPet) (D) grown in the presence of arabinose to overexpress SulA. Phase-contrast images (in red) were merged with fluorescent images (in green). The graphs beside each panel represent the plot of differential fluorescence intensities between the left side and right side of each cell, calculated for 5 representative cells of each strain, chosen from fields of view containing >100 cells. Mean values are reported, with scale bars representing the standard deviations from the means. Cells were grown in M9 medium supplemented with 0.2% glycerol at 37°C, and 0.2% arabinose was added for one generation before imaging was performed. Bars, 2 $\mu$m.

inhibitory effect of MinC. Addition of ZapA had no effect on the Min waves in the absence of FtsZ (data not shown). Upon addition of ZapA, the FtsZ bundles were no longer spatially regulated by the Min waves (Fig. 4A, bottom panel). We found that after ZapA addition, FtsZ bundles spread upon the lipid surface (Fig. 4A, bottom panel) and occupied the gaps left by the dispersing Min waves on the lipid bilayer (Fig. 4B). These results indicate that FtsZ bundling caused by ZapA protects FtsZ bundles from the inhibitory effect of MinC under these minimal *in vitro* conditions. The disappearance of visible Min waves upon ZapA addition is likely to be due to the increased stability of FtsZ bundles, which, instead of disassembling due to Min waves, stably assembled and occupied the available surface on the membrane, disrupting the Min waves.

To further investigate the effect of ZapA on FtsZ assembly, fluorescence recovery after photobleaching (FRAP) was used to measure the effect of ZapA on FtsZ turnover on the lipid bilayers. We found that ZapA inhibited FtsZ turnover in a concentration-dependent manner (Fig. 4C). In the absence of ZapA, the value for the turnover rate of FtsZ (the half-time of recovery of the bleached FtsZ-YFP-MTS region on the lipid bilayer) was about 10 s (Fig. 4C; see the supplemental material for turnover rate calculation). Upon ZapA addition, this value increased to 12 and 14 s in the presence of 0.1 $\mu$m and 0.2 $\mu$m ZapA, respectively (Fig. 4C). In addition, the mobile fraction of FtsZ (the fraction of total FtsZ actively showing turnover between filaments and solution) was 94% in the absence of ZapA and was reduced to 76% and 52% in the presence of 0.1 $\mu$m and 0.2 $\mu$m ZapA, respectively, confirming the inhibitory effect of ZapA on FtsZ turnover (see the supplemental material for details on calculations).

GTP hydrolysis, although not required for FtsZ protofilament assembly (43, 44), is required for FtsZ turnover, as it appears to provide a way to destabilize the polymers, leading to constant exchange of FtsZ subunits (37). ZapA has been shown to inhibit FtsZ GTPase activity, likely as a consequence of enhanced lateral association of FtsZ protofilaments (21, 22). Since GTP hydrolysis is the rate-limiting factor for depolymerization of FtsZ (45), we suggest that the effect of ZapA on FtsZ turnover is linked to reduced GTPase activity of FtsZ. The sensitivity of FtsZ to MinC was shown to be critically dependent on the GTPase activity of FtsZ (6, 37). More-recent work suggests that it is the hydrolysis-induced turnover that is utilized by MinC to depolymerize FtsZ (6). Our data provide direct support for the view that ZapA may protect FtsZ from MinC by reducing FtsZ turnover, as shown in the model (Fig. 4D).

We have been unable to recapitulate the *in vitro* protection of FtsZ bundles from MinC action in our *in vivo* assays, either because of the insensitivity of the assays or because other *in vivo* factors influence the stability of FtsZ bundles and/or the effect of ZapA on them.

The rate of FtsZ turnover measured here in the *in vitro* assays is similar to that estimated by *in vivo* FRAP (9 s) (38) and to the rate of exchange of FtsZ subunits between protofilaments (which is indicative of the rate of assembly of FtsZ protofilaments) calcu-

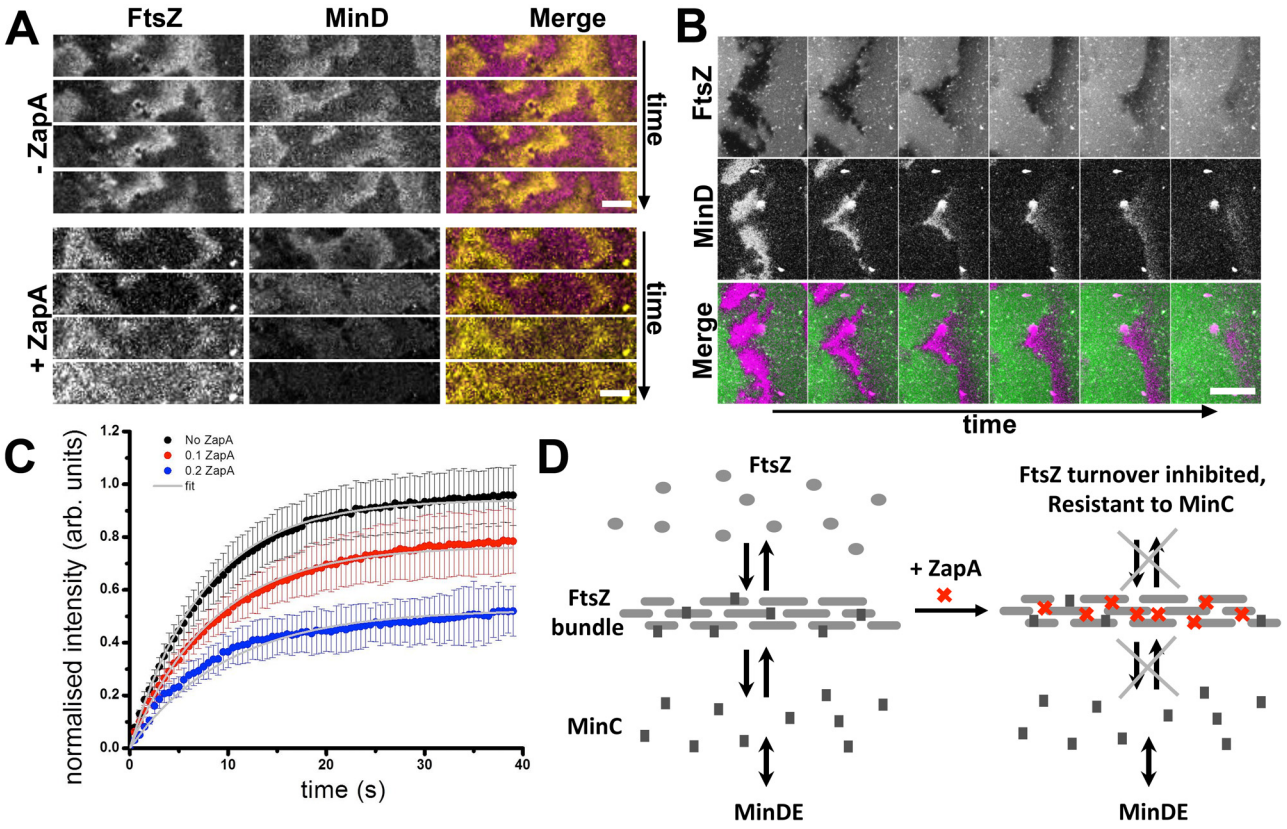


**FIG 4** Effect of ZapA on FtsZ-Min waves reconstituted on supported lipid bilayers. (A) Time-lapse analysis of reconstituted FtsZ-Min waves in the absence (top panel) and in the presence (bottom panel) of ZapA. Images were acquired every 30 s. FtsZ was visualized thanks to the presence of 50% fluorescently labeled FtsZ-YFP-MTS; similarly, MinD was present as a mixture of unlabeled and 20% labeled MinD-Cy5. Adding ZapA resulted in disruption of both FtsZ and MinD waves. Bar, 25 $\mu$m. (B) A more detailed version of the experiment reported for panel A, performed in the presence of ZapA. FtsZ bundling caused by ZapA resulted in stable FtsZ assembly in areas previously occupied by Min waves, which disappeared. Scale bar, 50 $\mu$m. (C) FRAP performed on FtsZ bundles assembled on supported lipid bilayers. The graph reports the recovery of the intensity of FtsZ-YFP-MTS fluorescence after photobleaching, in the presence of different concentrations of ZapA. The *y* axis represents the range of intensities of recovery after photobleaching. Curves were fitted with a reaction-dominant model as described in the supplemental material. arb., arbitrary. (D) Model explaining the effect of ZapA on FtsZ bundles and the consequence of its coupling to the Min waves. FtsZ bundles exhibit GTPase-induced turnover. This turnover is essential for the action of MinC, which results in coupling of FtsZ polymerization to the Min waves. In the presence of ZapA, which is known to bundle FtsZ polymers and to inhibit FtsZ GTPase activity, the FtsZ bundles are rendered resistant to MinC, thus decoupling them from the Min waves.

lated by *in vitro* FRET analysis (3.5 to 7 s) (46). These values are all consistent with our model for the counter-oscillation of FtsZ-bound ZapAB and ZipA, which requires not only that FtsZ be able to rapidly assemble into bundles at the cell pole with the lowest MinC concentration but that bundle disassembly also occurs sufficiently rapidly when MinC is present, thereby supporting an oscillation (and counter-oscillation) period of about 20 s.

**Conclusions.** In this work, we have shown that early-cell-division proteins display highly dynamic behavior prior to septum formation. We have shown a co-oscillation of ZipA, ZapAB, and FtsZ from pole to pole which is in the direction opposite to that of MinCDE, has the same period, and is dependent on functional MinCDE and FtsZ polymerization. These results lead us to propose that FtsZ rapidly assembles into slowly diffusing protofilaments and bundles, is tethered to the cell membrane through FtsA or ZipA, and is limited in length by the combined action of the Min and the nucleoid occlusion systems, as proposed by Pichoff and Lutkenhaus (47). Our results indicate that these slowly diffusing bundles accumulate at the cell pole where the MinC concentration is lowest and are bound by ZipA and ZapAB, thereby allowing their visualization at the timescales assayed. As a wave of MinC approaches these complexes, disassembly to give rapidly diffusing complexes occurs rapidly, thereby leading to the apparent counter-oscillation. This behavior was recapitulated in an *in vitro* system that showed that FtsZ bundles are excluded from dynamic Min waves. The ability of FtsZ oligomers to begin the physical association with ZapA, ZapB, and ZipA prior to septum formation represents an efficient mechanism for a rapid assembly of the divisome once targeting to the cell center can occur as a consequence of the completion of chromosome segregation.

## MATERIALS AND METHODS

**Bacterial strains.** All strains used in this work were derivatives of *E. coli* K-12 AB1157 (48) and are listed in Table 1. Strains containing a C-terminal fluorescent fusion of ZipA to YPet or to mCherry were constructed by λ-Red recombination essentially as described before (49) using oligonucleotides ZipA-F and ZipA-R and selecting for kanamycin resistance (Kan$^r$). Strains containing YPet-ZapA, mCherry-ZapA, YPet-

**TABLE 1** List of strains used in this work

| Strain | Genotype (phenotype) | Source |
|---|---|---|
| PB131 | *yPet-zapA* (Km$^r$) *zipA-mCherry frt* | This study |
| PB206 | *yPet-minC* (Km$^r$) | This study |
| PB208 | *yPet-zapA* (Km$^r$) *zipA-mCherry frt* $p_{ftsK}$ *ftsZ-cfp* (Amp$^r$) | This study |
| PB211 | *yPet-minC* (Km$^r$) *zipA-mCherry frt* | This study |
| PB213 | *yPet-minC* (Km$^r$) *mCherry-zapA frt* | This study |
| PB220 | *yPet-zapA* (Km$^r$) *zipA-mCherry frt* Δ*minDE* (Tet$^r$) | This study |
| PB230 | $p_{ftsK}$ *ftsZ-cfp* (Amp$^r$) | This study |
| PB240 | *yPet-zapA frt* $p_{ftsK}$ *ftsZ-cfp* (Amp$^r$) | This study |
| PB245 | *yPet-zapA frt* $p_{ara}$ *sulA* (Cm$^r$) | This study |
| PB253 | $p_{ftsK}$ *ftsZ-cfp* (Amp$^r$) $p_{ara}$*sulA* (Cm$^r$) | This study |
| PB283 | *zipA-yPet* (Km$^r$) $p_{ftsK}$ *ftsZ-cfp* (Amp$^r$) | This study |
| PB318 | *mCherry-minC* (Km$^r$) *yPet-zapB frt* | This study |
| PB319 | *mCherry-zapA* (Km$^r$) *yPet-zapB frt* | This study |
| PB323 | *yPet-zapB frt* $p_{ara}$*sulA* (Cm$^r$) | This study |
| PB325 | *yPet-zapB frt* $p_{ftsK}$ *ftsZ-cfp* (Amp$^r$) | This study |
| PB333 | *mCherry-zapA* (Km$^r$) *yPet-zapB frt* $p_{ftsK}$ *ftsZ-cfp* (Amp$^r$) | This study |
| PB334 | *zipA-mCherry* (Km$^r$) *yPet-zapB frt* $p_{ftsK}$ *ftsZ-cfp* (Amp$^r$) | This study |
| PB351 | *mCherry-zapA frt yPet-zapB frt* Δ*minDE* (Tet$^r$) | This study |
| PB352 | *zipA-mCherry frt yPet-zapB frt* Δ*minDE* (Tet$^r$) | This study |
| PB393 | *yPet-zapB frt* $p_{ftsK}$ *ftsZ-cfp* (Amp$^r$) Δ*zapA* (Cm$^r$) | This study |
| PB394 | *zipA-yPet* (Km$^r$) $p_{ara}$*sulA* (Cm$^r$) | This study |

ZapB, YPet-MinC, and mCherry-MinC N-terminal fluorescent derivatives were constructed by λ-Red recombination using oligonucleotide pair ZapA-NF and ZapA-NR, oligonucleotide pair ZapB-NF and ZapB-NR, and oligonucleotide pair MinC-NF and MinC-NR selecting for kanamycin resistance. Oligonucleotides used in this work are presented in Table S1 in the supplemental material. When required, the DNA region between the two *frt* sites containing the kanamycin resistance gene of these strains was removed using Flp recombinase expressed from pCP20 (50). Strains containing two fluorescent derivatives of ZapA, ZapB, or ZipA were constructed by P1 transduction, using a strain containing one of the constructs as the donor strain and a strain containing the other construct as the receiver strain, selecting for kanamycin resistance. Strains expressing an FtsZ-CFP fluorescent derivative contain plasmid pCP8, which allows constitutive expression of FtsZ-CFP from a weak promoter and provides ampicillin resistance (Amp$^r$) (32). Strains expressing SulA under conditions of arabinose-inducible control were constructed by transformation with plasmid pWM1736, a kind gift from William Margolin (34), selecting for chloramphenicol resistance (Cm$^r$). Strains deleted for *minDE* and *zapA* were constructed by P1 transduction using strain WX0 (AB1157 Δ*minDE* Tet$^r$; laboratory stock) and strain HY1-31 (MC4100 Δ*zapA* Cm$^r$; a kind gift from Anuradha Janakiraman [51]) as donor strains, selecting for tetracycline resistance (Tet$^r$) and chloramphenicol resistance, respectively.

**Preparation of cells for microscopy.** Cells were grown at 37°C and 220 rpm in LB until the early exponential phase and then subcultured overnight in M9 glycerol. The following day, cultures with an $A_{600}$ of between 0.1 and 0.4 were diluted to an $A_{600}$ of 0.02 and grown until an $A_{600}$ of 0.1 was achieved. Newborn cells were 2.2 to 2.5 μm long, and dividing cells were 4.4 to 5.0 μm long. Cells were then concentrated and laid on an M9–glycerol–1% agarose pad. For nucleoid visualization, cells were stained with 1 μg ml$^{-1}$ DAPI (4′,6-diamidino-2-phenylindole) immediately before imaging was performed. For SulA overexpression, 0.2% arabinose was added to exponentially growing cultures at an $A_{600}$ of 0.1 for one generation before imaging was performed.

**Image acquisition and analysis.** Cells were visualized with a 100× objective on a Nikon Eclipse TE2000-U microscope, equipped with a Photometrics Cool-SNAP HQ charge-coupled-device (CCD) camera and a temperature-controlled incubation chamber, at the constant temperature of 37°C. Images were acquired and analyzed using Metamorph 6.2 software and ImageJ. Reconstituted FtsZ-Min waves were visualized using a Zeiss LSM 780 confocal microscope with a Zeiss 40 × 1.2 numerical aperture (NA) objective. The same equipment was used for the photobleaching experiments. Analysis of fluorescence dynamics and oscillations was performed precisely as described in reference 34: in order to calculate the fluorescent intensity differential in time-lapse experiments, the levels of integrated fluorescence over the left half and right half of each analyzed cell were measured at each time point, and the differences between these values (right half minus left half) were calculated and plotted in a graph against time.

**Protein purification.** His-MinD and His-MinE were purified and fluorescently labeled as previously described (39, 41). His-eGFP-MinC was purified as previously described (41), with an extra size exclusion chromatography step. *E. coli* FtsZ-YFP-MTS, FtsZ-F268C, and FtsZ were purified as described elsewhere (52). For a description of the FtsZ-YFP-MTS construct, see reference 52. ZapA was purified by nickel affinity column chromatography, with elution in imidazole. This was followed by dialysis and a second nickel column chromatography procedure with cleavage and elution of ZapA without a His tag with factor Xa (Novogen).

**Supported lipid bilayers.** Small unilamellar vesicles (SUVs) were prepared by sonication of *E. coli* lipid extract (Avanti Lipids) (4 mg ml$^{-1}$) with 0.1 moles percent (mol%) DiI in FtsZ polymerization buffer at room temperature. The suspension was diluted to 0.5 mg ml$^{-1}$ and added to the substrates or glass rods and warmed to 37°C. Adding $CaCl_2$ to a 2.5 mM concentration induced fusion of the SUVs on mica, leading to bilayer formation. The sample was rinsed with 2 ml polymerization buffer to remove unfused SUVs.

**Protein assemblies and assays.** For reconstitution of MinCDE waves and FtsZ filaments, a Tris buffer (50 mM Tris [pH 7.5], 150 mM NaCl, 7.5 mM $MgCl_2$) was used. The final FtsZ concentration used for FRAP, single-molecule, and depolymerization experiments was 0.2 μM. To perform FRAP, FtsZ filament networks were assembled with 1:1 FtsZ and FtsZ-YFP-MTS at 0.2 μM in Tris buffer. Different concentrations of ZapA were added and allowed to equilibrate for 5 min before FRAP was performed on a total internal reflectance fluorescence (TIRF) microscope. FRAP curves were analyzed by ImageJ, and fitting was done using OriginLab with a reaction dominant model as explained in the supplemental material. For reconstitution of the waves, the total concentrations of the proteins used were 1 μM MinD, 1.5 μM MinE, 0.2 μM MinC, and 1 μM FtsZ. MinD was doped with 20 mol% MinD-Cy5 and FtsZ with 50 mol% FtsZ-YFP-MTS. GTP and ATP were used at 500 μM each. ZapA was added to a concentration of 0.1 μM. All the buffers in the experimental chamber were supplemented with an oxygen-scavenging system consisting of glucose oxidase (75 U ml$^{-1}$), catalase (1,500 U ml$^{-1}$), β-D-glucose (0.25 [wt/vol]), and trolox (6-hydroxy-2,5,7,8-tetramethylchroman-2-carboxylic acid) (1 mM) just before the experiments were performed. FRAP curves were analyzed by ImageJ, and fitting was done using OriginLab and a reaction-dominant model as explained in the supplemental material.

## SUPPLEMENTAL MATERIAL

Supplemental material for this article may be found at http://mbio.asm.org/lookup/suppl/doi:10.1128/mBio.00856-13/-/DCSupplemental.

Text S1, DOCX file, 0.1 MB.
Figure S1, PDF file, 0.7 MB.
Figure S2, PDF file, 0.6 MB.
Figure S3, PDF file, 0.5 MB.
Figure S4, PDF file, 0.6 MB.
Table S1, DOCX file, 0.1 MB.
Movie S1, AVI file, 2 MB.
Movie S2, AVI file, 0.2 MB.
Movie S3, AVI file, 0.6 MB.

## ACKNOWLEDGMENTS

We thank William Margolin for the kind gift of plasmid pWM1736, Anuradha Janakiraman for the kind gift of strain HY1-31, and Jakob Schweizer for useful discussion.

The work was supported by an ESF-BBSRC (BB/I004785/1) grant to D.S. and an (ESF) (SCHW716/7-1) grant to P.S. and by the Dresden International PhD Program for Biomedicine and Bioengineering fellowship to S.A.

## REFERENCES

1. **Lutkenhaus J, Pichoff S, Du S.** 2012. Bacterial cytokinesis: from Z ring to divisome. Cytoskeleton (Hoboken) **69:**778–790.
2. **Bernhardt TG, de Boer PA.** 2005. SlmA, a nucleoid-associated, FtsZ binding protein required for blocking septal ring assembly over chromosomes in *E. coli*. Mol. Cell **18:**555–564.
3. **Cho H, McManus HR, Dove SL, Bernhardt TG.** 2011. Nucleoid occlusion factor SlmA is a DNA-activated FtsZ polymerization antagonist. Proc. Natl. Acad. Sci. U. S. A. **108:**3773–3778.
4. **Tonthat NK, Arold ST, Pickering BF, Van Dyke MW, Liang S, Lu Y, Beuria TK, Margolin W, Schumacher MA.** 2011. Molecular mechanism by which the nucleoid occlusion factor, SlmA, keeps cytokinesis in check. EMBO J. **30:**154–164.
5. **Hu Z, Mukherjee A, Pichoff S, Lutkenhaus J.** 1999. The MinC component of the division site selection system in Escherichia coli interacts with FtsZ to prevent polymerization. Proc. Natl. Acad. Sci. U. S. A. **96:**14819–14824.
6. **Dajkovic A, Lan G, Sun SX, Wirtz D, Lutkenhaus J.** 2008. MinC spatially controls bacterial cytokinesis by antagonizing the scaffolding function of FtsZ. Curr. Biol. **18:**235–244.
7. **Shen B, Lutkenhaus J.** 2010. Examination of the interaction between FtsZ and MinCN in *E. coli* suggests how MinC disrupts Z rings. Mol. Microbiol. **75:**1285–1298.
8. **Hernández-Rocamora VM, García-Montañés C, Reija B, Monterroso B, Margolin W, Alfonso C, Zorrilla S, Rivas G.** 2013. MinC protein shortens FtsZ protofilaments by preferentially interacting with GDP-bound subunits. J. Biol. Chem. **288:**24625–24635.
9. **Lutkenhaus J.** 2007. Assembly dynamics of the bacterial MinCDE system and spatial regulation of the Z ring. Annu. Rev. Biochem. **76:**539–562.
10. **Meinhardt H, de Boer PA.** 2001. Pattern formation in *Escherichia coli*: a model for the pole-to-pole oscillations of Min proteins and the localization of the division site. Proc. Natl. Acad. Sci. U. S. A. **98:**14202–14207.
11. **de Boer PA.** 2010. Advances in understanding *E. coli* cell fission. Curr. Opin. Microbiol. **13:**730–737.
12. **Goehring NW, Beckwith J.** 2005. Diverse paths to midcell: assembly of the bacterial cell division machinery. Curr. Biol. **15:**R514–R526.
13. **Weiss DS.** 2004. Bacterial cell division and the septal ring. Mol. Microbiol. **54:**588–597.
14. **Aarsman ME, Piette A, Fraipont C, Vinkenvleugel TM, Nguyen-Distèche M, den Blaauwen T.** 2005. Maturation of the *Escherichia coli* divisome occurs in two steps. Mol. Microbiol. **55:**1631–1645.
15. **Hale CA, de Boer PA.** 1999. Recruitment of ZipA to the septal ring of *Escherichia coli* is dependent on FtsZ and independent of FtsA. J. Bacteriol. **181:**167–176.
16. **Hale CA, Rhee AC, de Boer PA.** 2000. ZipA-induced bundling of FtsZ polymers mediated by an interaction between C-terminal domains. J. Bacteriol. **182:**5153–5166.
17. **Mateos-Gil P, Márquez I, López-Navajas P, Jiménez M, Vicente M, Mingorance J, Rivas G, Vélez M.** 2012. FtsZ polymers bound to lipid bilayers through ZipA form dynamic two dimensional networks. Biochim. Biophys. Acta **1818:**806–813.
18. **Pazos M, Natale P, Vicente M.** 2013. A specific role for the ZipA protein in cell division: stabilization of the FtsZ protein. J. Biol. Chem. **288:**3219–3226.
19. **Gueiros-Filho FJ, Losick R.** 2002. A widely conserved bacterial cell division protein that promotes assembly of the tubulin-like protein FtsZ. Genes Dev. **16:**2544–2556.
20. **Low HH, Moncrieffe MC, Löwe J.** 2004. The crystal structure of ZapA and its modulation of FtsZ polymerisation. J. Mol. Biol. **341:**839–852.
21. **Small E, Marrington R, Rodger A, Scott DJ, Sloan K, Roper D, Dafforn TR, Addinall SG.** 2007. FtsZ polymer-bundling by the *Escherichia coli* ZapA orthologue, YgfE, involves a conformational change in bound GTP. J. Mol. Biol. **369:**210–221.
22. **Mohammadi T, Ploeger GE, Verheul J, Comvalius AD, Martos A, Alfonso C, van Marle J, Rivas G, den Blaauwen T.** 2009. The GTPase activity of *Escherichia coli* FtsZ determines the magnitude of the FtsZ polymer bundling by ZapA *in vitro*. Biochemistry **48:**11056–11066.
23. **Dajkovic A, Pichoff S, Lutkenhaus J, Wirtz D.** 2010. Cross-linking FtsZ polymers into coherent Z rings. Mol. Microbiol. **78:**651–668.
24. **Galli E, Gerdes K.** 2010. Spatial resolution of two bacterial cell division proteins: ZapA recruits ZapB to the inner face of the Z-ring. Mol. Microbiol. **76:**1514–1526.
25. **Ebersbach G, Galli E, Møller-Jensen J, Löwe J, Gerdes K.** 2008. Novel coiled-coil cell division factor ZapB stimulates Z ring assembly and cell division. Mol. Microbiol. **68:**720–735.
26. **Mercier R, Petit MA, Schbath S, Robin S, El Karoui M, Boccard F, Espéli O.** 2008. The MatP/matS site-specific system organizes the terminus region of the *E. coli* chromosome into a macrodomain. Cell **135:**475–485.
27. **Espéli O, Borne R, Dupaigne P, Thiel A, Gigant E, Mercier R, Boccard F.** 2012. A MatP-divisome interaction coordinates chromosome segregation with cell division in *E. coli*. EMBO J. **31:**3198–3211.
28. **Wang X, Huang J, Mukherjee A, Cao C, Lutkenhaus J.** 1997. Analysis of the interaction of FtsZ with itself, GTP, and FtsA. J. Bacteriol. **179:**5551–5559.
29. **Den Blaauwen T, Buddelmeijer N, Aarsman ME, Hameete CM, Nanninga N.** 1999. Timing of FtsZ assembly in *Escherichia coli*. J. Bacteriol. **181:**5167–5175.
30. **Rueda S, Vicente M, Mingorance J.** 2003. Concentration and assembly of the division ring proteins FtsZ, FtsA, and ZipA during the *Escherichia coli* cell cycle. J. Bacteriol. **185:**3344–3351.
31. **Galli E, Gerdes K.** 2012. FtsZ-ZapA-ZapB interactome of *Escherichia coli*. J. Bacteriol. **194:**292–302.
32. **Wang X, Possoz C, Sherratt DJ.** 2005. Dancing around the divisome: asymmetric chromosome segregation in *Escherichia coli*. Genes Dev. **19:**2367–2377.
33. **Juarez JR, Margolin W.** 2010. Changes in the Min oscillation pattern before and after cell birth. J. Bacteriol. **192:**4134–4142.
34. **Thanedar S, Margolin W.** 2004. FtsZ exhibits rapid movement and oscillation waves in helix-like patterns in *Escherichia coli*. Curr. Biol. **14:**1167–1173.
35. **Cordell SC, Robinson EJ, Lowe J.** 2003. Crystal structure of the SOS cell division inhibitor SulA and in complex with FtsZ. Proc. Natl. Acad. Sci. U. S. A. **100:**7889–7894.
36. **Dajkovic A, Mukherjee A, Lutkenhaus J.** 2008. Investigation of regulation of FtsZ assembly by SulA and development of a model for FtsZ polymerization. J. Bacteriol. **190:**2513–2526.
37. **Erickson HP, Anderson DE, Osawa M.** 2010. FtsZ in bacterial cytokinesis: cytoskeleton and force generator all in one. Microbiol. Mol. Biol. Rev. **74:**504–528.
38. **Anderson DE, Gueiros-Filho FJ, Erickson HP.** 2004. Assembly dynamics of FtsZ rings in *Bacillus subtilis* and *Escherichia coli* and effects of FtsZ-regulating proteins. J. Bacteriol. **186:**5775–5781.
39. **Loose M, Fischer-Friedrich E, Ries J, Kruse K, Schwille P.** 2008. Spatial regulators for bacterial cell division self-organize into surface waves *in vitro*. Science **320:**789–792.
40. **Arumugam S, Chwastek G, Fischer-Friedrich E, Ehrig C, Mönch I, Schwille P.** 2012. Surface topology engineering of membranes for the mechanical investigation of the tubulin homologue FtsZ. Angew. Chem. Int. Ed. Engl. **19:**11858–11862.
41. **Loose M, Fischer-Friedrich E, Herold C, Kruse K, Schwille P.** 2011. Min protein patterns emerge from rapid rebinding and membrane interaction of MinE. Nat. Struct. Mol. Biol. **18:**577–583.
42. **Scheffers DJ.** 2008. The effect of MinC on FtsZ polymerization is pH dependent and can be counteracted by ZapA. FEBS Lett. **582:**2601–2608.
43. **Chen Y, Bjornson K, Redick SD, Erickson HP.** 2005. A rapid fluorescence assay for FtsZ assembly indicates cooperative assembly with a dimer nucleus. Biophys. J. **88:**505–514.
44. **Mukherjee A, Lutkenhaus J.** 1998. Dynamic assembly of FtsZ regulated by GTP hydrolysis. EMBO J. **17:**462–469.
45. **Romberg L, Mitchison TJ.** 2004. Rate-limiting guanosine 5′-

triphosphate hydrolysis during nucleotide turnover by FtsZ, a prokaryotic tubulin homologue involved in bacterial cell division. Biochemistry **43:** 282–288.

46. **Chen Y, Erickson HP.** 2009. FtsZ filament dynamics at steady state: subunit exchange with and without nucleotide hydrolysis. Biochemistry **48:**6664–6673.
47. **Pichoff S, Lutkenhaus J.** 2005. Tethering the Z ring to the membrane through a conserved membrane targeting sequence in FtsA. Mol. Microbiol. **55:**1722–1734.
48. **Bachmann BJ.** 1972. Pedigrees of some mutant strains of *Escherichia coli* K-12. Bacteriol. Rev. **36:**525–557.
49. **Reyes-Lamothe R, Sherratt DJ, Leake MC.** 2010. Stoichiometry and architecture of active DNA replication machinery in *Escherichia coli*. Science **328:**498–501.
50. **Datsenko KA, Wanner BL.** 2000. One-step inactivation of chromosomal genes in *Escherichia coli* K-12 using PCR products. Proc. Natl. Acad. Sci. U. S. A. **97:**6640–6645.
51. **Durand-Heredia JM, Yu HH, De Carlo S, Lesser CF, Janakiraman A.** 2011. Identification and characterization of ZapC, a stabilizer of the FtsZ ring in *Escherichia coli*. J. Bacteriol. **193:**1405–1413.
52. **Osawa M, Anderson DE, Erickson HP.** 2008. Reconstitution of contractile FtsZ rings in liposomes. Science **320:**792–794.